A more precise mass measurement of the Λ_c baryon with the LHCb experiment

Carter Eikenbary
Supervisor: Dr. Michael Sokoloff
Physics Capstone

Abstract

This research project presents a precision mass measurement of the Λ_c baryon. The study focuses on the three-body decay mode, $\Lambda_c^+ \to pK^+K^-$. The analysis utilizes data with 1.6 fb^{-1} of integrated luminosity collected by the LHCb collaboration in 2017 during the Run II period of the LHC. After setting requirements on the final-state particles and the decay kinematics, the Λ_c mass was measured to be $228x.xx \pm 0.06865\,\text{MeV}/c^2$. A large source of systematic error was found by studying how the Λ_c mass measurement depends on the magnetic field orientation within the LHCb detector. After applying correction factors to the final-state particle's momentum, the systematic uncertainty corresponding to the magnetic field orientation became consistent with statistical fluctuation. This reduction in systematic error resulted in a Λ_c mass measurement of $228x.xx \pm 0.04969\,\text{MeV}/c^2$.

Contents

1 Introduction

Since the 1970s, the Standard Model of particle physics has shaped our understanding of how elementary particles interact. Shown in Figure 1 is the Standard Model, which distinguishes elementary particles into two distinct families, fermions and bosons. Fermions are the building blocks of matter, and bosons are the mediators of force interactions. Fermions of particular interest to particle physics research are known as quarks. Quarks must be bound to other quarks by the strong nuclear force. The particles composed of multiple quarks are known as hadrons. Baryons are hadrons composed of three quarks or anti-quarks and mesons are composed of a quark/antiquark pair. The LHCb collaboration studies the decays of hadrons containing charm quarks and anti-quarks to understand the asymmetries between matter and antimatter known as CP violation. One of the charm hadrons of particular interest is the Λ_c baryon because it, and its antiparticle, can be created in abundance from the proton-proton collisions within the Large Hadron Collider. The Λ_c baryon is a particle composed of an up, down, and charm quark. A precision study of the Λ_c baryon will provide essential details for understanding CP violation. Furthermore, the LHCb collaboration has recently discovered doubly charmed baryons that decay into the Λ_c baryon. Precision measurements of the Λ_c mass can help with determining kinematic constraints for doubly charmed baryons.

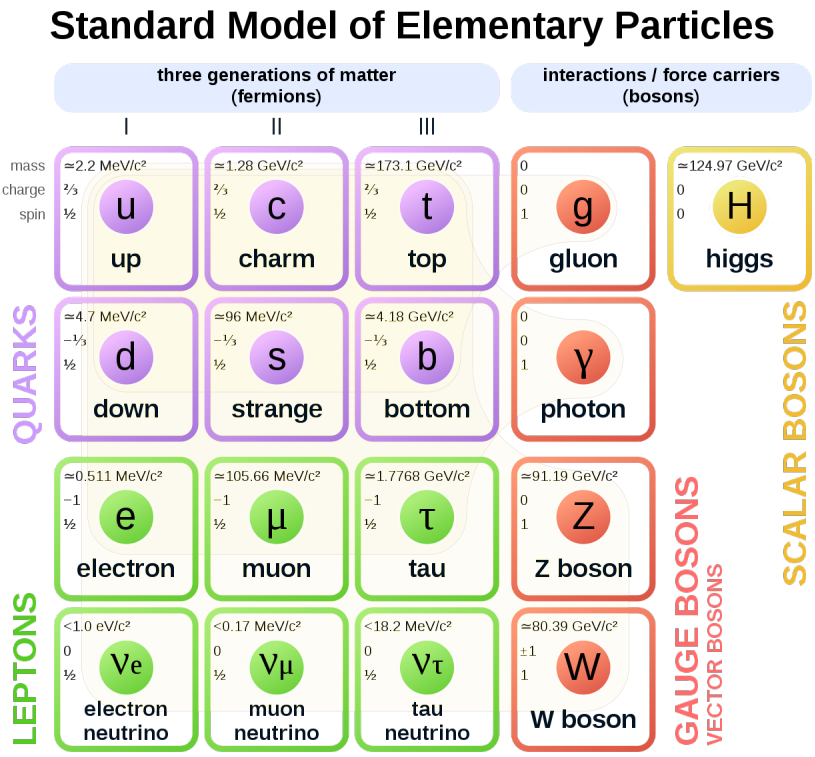

Figure 1: Standard Model of particle physics (From [8]).

2 LHCb Detector

Buried far beneath the France-Switzerland border sits the Large Hadron Collider (LHC), the world's largest and highest-energy particle accelerator. The LHC can generate a tremendous amount of data by colliding two 6.5 TeV proton beams 1 billion times a second [2]. These proton-proton collisions occur at multiple points within the particle accelerator. At one of these collision points is the Large Hadron Collider beauty (LHCb) detector. The LHCb detector is a single-arm forward spectrometer dedicated to observing the creation and decays of hadrons containing beauty and charm quarks. Beauty and charm hadrons produced by the collision will have forward momentum and stay close to the beam line. By colliding the proton-proton beams at the front, particles created from beauty and charm hadron decays will pass through the various LHCb sub-detectors. Shown in Figure 2 is a side-view of the LHCb detector with the various sub-detectors. The first of these sub-detectors is the Vertex Locator (VELO). The VELO specializes in identifying locations of proton-proton collisions and determining decay vertices for beauty and charm hadrons. Once hadrons exit the VELO, they enter a Ring Imaging Cherenkov (RICH) detector to receive identification probabilities. After RICH-1, hadrons pass through a silicon tracker (TT) that determines the hadron's initial trajectory. Then hadrons pass through a powerful dipole magnet that bends the hadron's path depending on their charge. The hadrons then pass through a series of three-tracker systems that determine the final trajectory and opening angle for each hadron. From this information, an indirect measurement of mass and momentum for each hadron is determined.

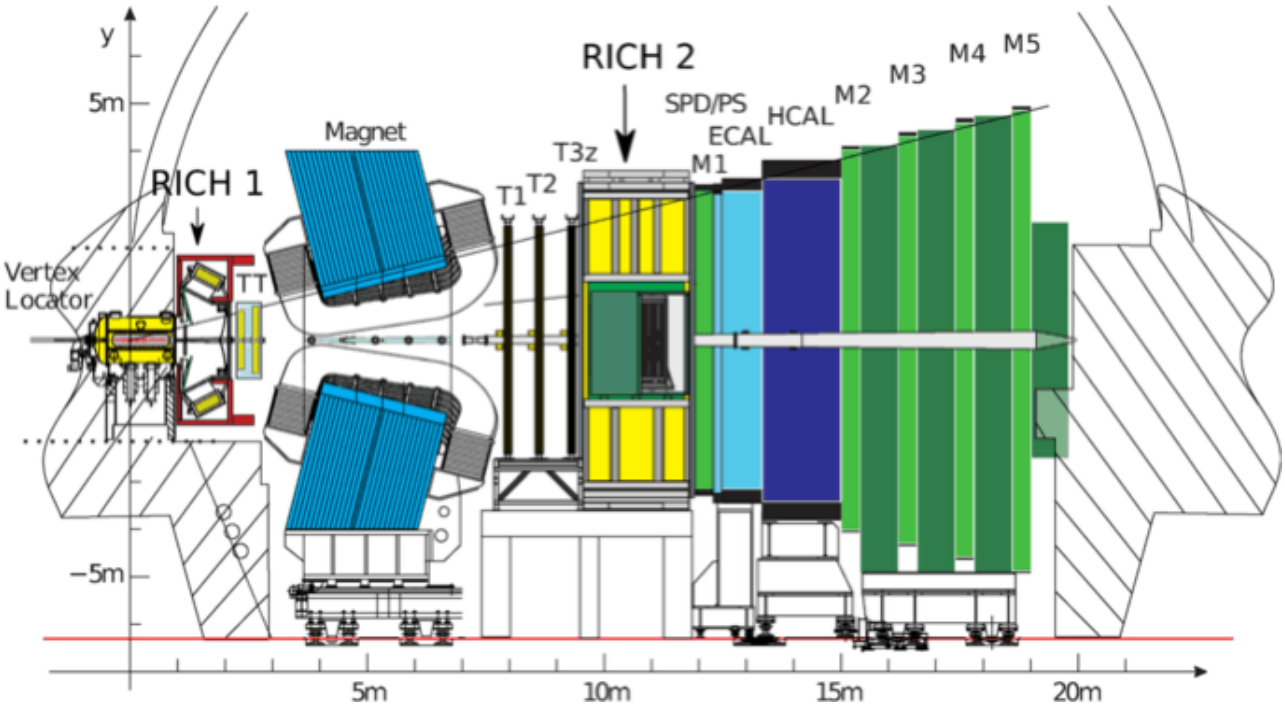

Figure 2: LHCb detector with the sub-detectors labeled (From [4]).

3 Data Sample

Our study of the Λ_c mass uses data samples collected during the Run II period of LHC in 2017. During the 2017 run year, the proton-proton collisions occurred with a center of mass energy of 13 TeV and integrated luminosity of 1.6 fb^{-1} [3]. At the LHCb, a month-long run period occurs in which the magnet polarity remains unchanged. Then, before the next run period, a brief shutdown occurs to change the magnet polarity. Therefore, data samples are separated into events collected during Magnet-Down and Magnet-Up run periods. Hadrons created at the proton-proton collision with enough forward momentum will pass through a series of sub-detectors inside the LHCb. These sub-detectors determine each hadron's trajectory through the LHCb and measures the hadron's mass and transverse momentum. The LHCb's software will then reconstruct particle decays from this information. For the $\Lambda_c^+ \to pK^+K^-$ decay, the software picks out bachelor protons and kaons to reconstruct an event. Each event that the software generates contains all the pertinent information needed for a mass analysis of the Λ_c decay. Once the LHCb generates an event, it will send the event's information to a trigger line that filters out undesirable events. Events that pass the trigger are digitized and combined into a data sample usable for analysis. Table 1 shows the number of events in the Magnet-Down and Magnet-Up data samples after passing trigger lines.

Year and Polarity	Events [M]
2017 *Mag-Down*	9.59
2017 *Mag-Up*	9.35

Table 1: Number of events in each data sample, in millions.

Particle	Naming Convention
Λ_c	Lc
p	Proton
K^+	Kplus
K^-	Kminus

Table 2: Naming convention of data samples.

Contained in our data samples are numerous variables related to the kinematics of our decay for each final-state hadron and the Λ_c baryon. Therefore, it is useful to set a naming convention to differentiate each of the hadrons. Table 2 shows the naming convention set for the $\Lambda_c^+ \to pK^+K^-$ datasets. Meaning that the variable Lc_M refers to the Λ_c mass, and Kminus_P refers to the K^- momentum. Figure 3 presents the Λ_c mass histogram of all 2017 events that pass the trigger line. The histogram shows a distribution with 260 bins and the mass range of $[2222, 2352]\,\text{MeV}/c^2$.

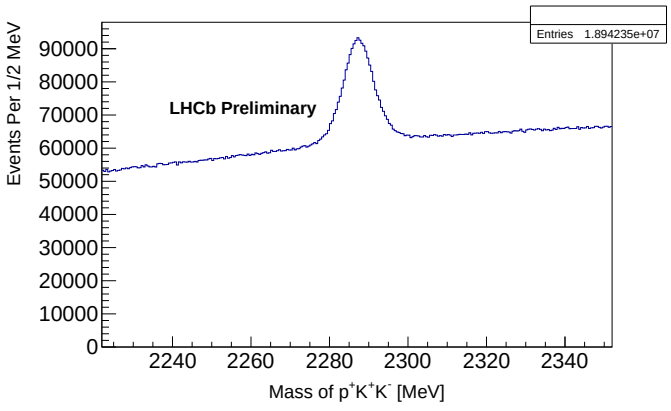

Figure 3: Λ_c mass histogram of all 2017 events that pass the trigger line selection.

4 Event Selection

4.1 PID selection

As a hadron passes through the LHCb, they interact with two Ring Imaging Cherenkov (RICH) sub-detectors. RICH detectors exploit the fact that the group velocity of light depends on the density of the medium it propagates through. When a charged hadron enters a RICH detector with a velocity greater than the speed of light for the medium, they emit a cone of photons known as Cherenkov radiation. RICH detectors can identify hadrons from the Cherenkov radiation they emit. The RICH detectors inside the LHCb detector have mirrors to collapse the cone of photons into a ring. By measuring a hadron's momentum and the radius of the photon ring it produces, we can accurately identify hadrons. The software assigns a probability to each charged track known as ProbNN when it reconstructs the event. These ProbNN variables use a neural network with adaptive training to measure the probability that a charged track is a specific hadron on a scale between $[0, 1]$. For example, ProbNNp measures the probability that a charged track was a proton. Protons will have a ProbNNp value close to one, whereas other hadrons will have ProbNNp values closer to zero. The LHCb has achieved exceptional performance at identifying hadrons by tuning the ProbNN variables with Monte Carlo simulations. Therefore we can discriminate events caused by misidentification by setting strict selection criteria, otherwise known as a cut, on these ProbNN variables. To determine an optimal ProbNN cut, we study the ProbNN distributions for signal events and background events to remove regions where there are more background events than signal events. We start by placing loose cuts on the ProbNN variables to properly assign regions of signal and background events in the Λ_c mass distribution. Monte Carlo simulations suggest that ProbNNp closely peaks near high probability for proton tracks. Therefore, this variable, along with a multiplication of the ProbNN variables for the three final-state hadrons, are great variables to remove events caused by misidentification. Shown in Table 3 are the preliminary cuts for these variables. Figure 2 shows the Λ_c mass histogram after applying the preliminary cuts from Table 3. There is a signal region from [2274,2300] MeV colored blue and two linear background regions on the far side-bands colored red. Events within the blue region will form the ProbNN signal distributions, and events within the red region will form the ProbNN background distributions.

PID Preliminary Cuts	
Variable	Cut
Product of ProbNN	> 0.4
Proton_ProbNNp	> 0.6

Table 3: Preliminary cuts for the PID variables. Product of ProbNN is the multiplication of Kplus_ProbNNk, Kminus_ProbNNk, and Proton_ProbNNp.

Figure 5 shows the signal and background distributions for the product of ProbNN for the three daughter hadrons and ProbNNp for the proton. The red distributions correspond to the events within the red background regions of Figure 2. Furthermore, the blue distributions correspond to the blue signal region of Figure 2. As a rough estimate, the background regions are linear, and the signal region models a Gaussian signal above a linear background. The red distributions will closely model the background within the signal region because the background distribution is approximately linear. Therefore, by subtracting the red ProbNN distributions from the blue ProbNN distributions, we can model a ProbNN distribution for purely signal events. Shown in Figure 5 are the purely signal region distributions displayed in green. To improve statistical precision, we want to cut regions where the red distribution dominates the green distribution. Table 4 shows the resulting cuts to improve the statistical precision.

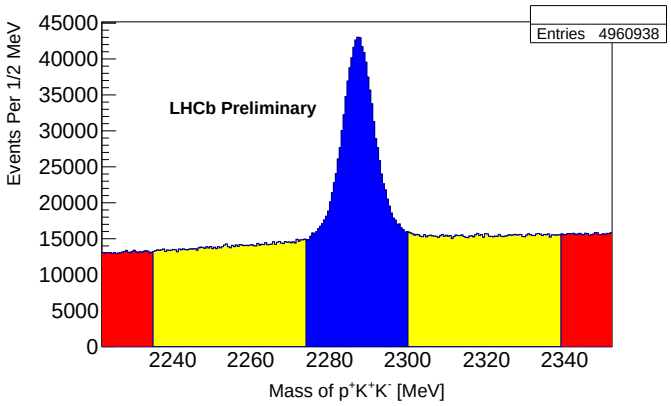

Figure 4: Λ_c mass after applying preliminary PID cuts. The red sections denotes the background regions and the blue denotes the signal region.

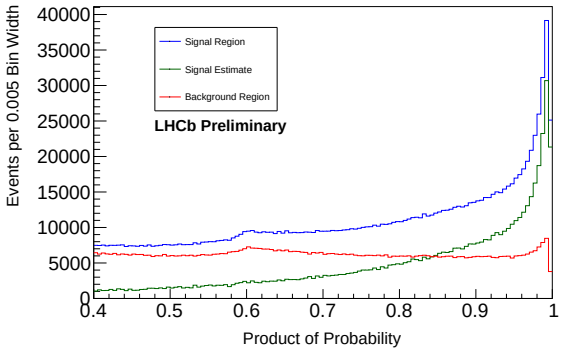

(a) Product of ProbNNx variables for the three final-state hadrons.

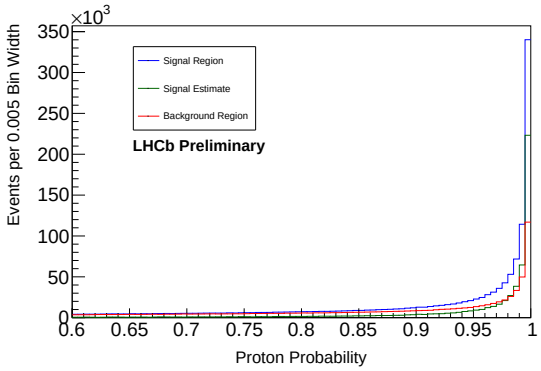

(b) ProbNNp variable for the proton.

Figure 5: ProbNN distributions for the signal region, shown in blue, and background regions, shown in red. Because the background is approximately linear we can subtract the background distribution from the signal distribution to estimate a purely signal distribution which is shown in green.

PID Cuts	
Variable	Cut
Product of ProbNNx	> 0.8
Proton_ProbNNp	> 0.9

Table 4: Final cuts for the PID variables after studying the signal and background distributions of ProbNN variables.

4.2 Phase-space selection

Now we are interested in restricting the kinematics of our three-body decay by setting selection criteria on the $\Lambda_c \to pK^+K^-$ phase-space. A visualization of the phase-space for a three-body decay is a Dalitz plot.

Richard Dalitz first used the Dalitz plot to study the decays $\tau^+ \to \pi^+\pi^-\pi^+$ and $\theta^+ \to \pi^+\pi^0$. At the time, τ^+ and θ^+ had the same mass and decay time. However, the final state of each decay suggests that the mesons have different parities. Particle theorists at the time believed that parity must be conserved. Therefore, the parity differences suggested that the τ^+ and θ^+ mesons were different particles. The Dalitz plot showed that the τ^+ and θ^+ mesons were the same particle, which we now call the K^+ meson, and the difference in parity was a result of parity violation in weak interactions. Dalitz plots are often used in modern particle physics to study the quantum mechanical resonances of final-state hadrons. Each event in the data set measures the momentum and energy of each particle. Thus we can construct Lorentz four-vectors for each final-state particle. Dalitz plots are constructed by adding the four-vectors of two particles and calculating the resulting vector's magnitude squared. This value is the squared mass when two particles are combined. Therefore, resonances on a Dalitz plot indicate that a large number of events involved an intermediate decay for two final-state particles. For the $\Lambda_c \to pK^+K^-$ decay, a resonance exists between the K^+ and K^- known as the $\phi(1020)$ meson. This means that the $\Lambda_c \to pK^+K^-$ decay could involve an intermediate decay $\Lambda_c \to p\phi$ and $\phi \to K^+K^-$. To determine the likelihood that the decay involved an intermediate ϕ meson, we can study the branching fractions for both decays. Branching fractions are the probability that a given particle will decay to a specific final state. The branching fraction for $\Lambda_c \to pK^+K^-$ without the $\phi(1020)$ decay is $(3.5 \pm 1.7) \times 10^{-4}\%$ and for $\Lambda_c \to p\phi$, the branching fraction is $(8.2 \pm 2.7) \times 10^{-4}\%$. Therefore, the $\Lambda_c \to p\phi$ intermediate decay is more than twice as likely to occur. Shown in Figure 6 is the Dalitz plot for $\Lambda_c^+ \to p^+K^+K^-$ events that pass the PID cuts. The x-axis is the squared magnitude of the K^+ and K^- four-vectors, and the y-axis is the squared magnitude of the p and K^- four-vectors. The Dalitz plot clearly shows a resonance between the K^+ and K^- mesons around 1.04 GeV^2/c^4, which is precisely the $\phi(1020)$ meson's mass squared. The $\phi(1020)$ resonance contains many events and exists in a small portion of the phase-space. Therefore, requiring that our decay involve the intermediate $\phi(1020)$ decay will remove a large amount of combinatorial background. Figure 6 also shows the magnitude squared distribution of the K^+ and K^- for signal and background events using the same method from section 4.1. There is a large signal-to-background ratio at the $\phi(1020)$ resonance. Therefore, our choice to require the intermediate $\phi(1020)$ is justified. Table 5 shows the selection criteria for the $\phi(1020)$ decay. We determined these cuts by using the PDG value of the $\phi(1020)$ mass squared and selecting a small window of 12 MeV above and below this value.

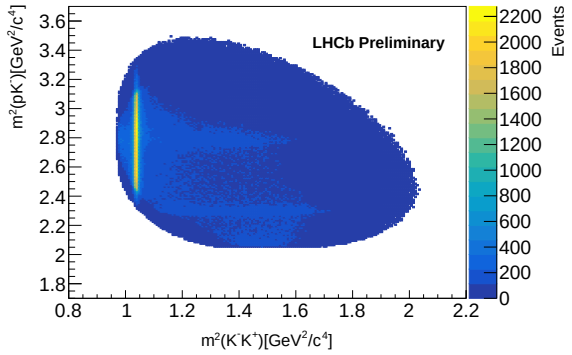

(a) Dalitz plot of $\Lambda_c^+ \to p^+K^+K^-$ decay.

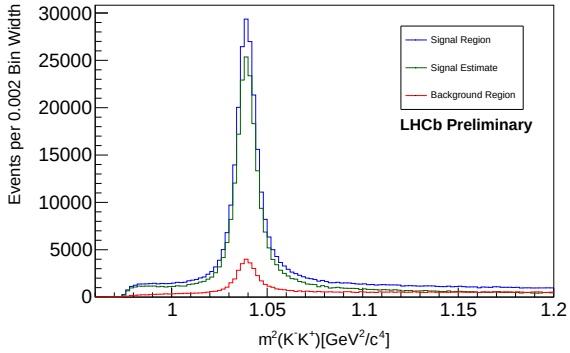

(b) Signal and background distributions of K^+K^- mass squared.

Figure 6: Large amounts of events are visible in both Figure4(a) and Figure4(b) around the $\phi(1020)$ mass squared region. Furthermore, Figure4(b) shows that the majority of these events are signal.

$\phi(1020)$ Cut	
Variable	Cut
m^2_ϕ	$> (1.019455 - 0.012)^2$ $[GeV^2/c^4]$
m^2_ϕ	$< (1.019455 + 0.012)^2$ $[GeV^2/c^4]$

Table 5: Cuts that require the $\Lambda_c^+ \to p^+K^+K^-$ to also include an intermediate $\phi(1020)$ decay.

4.3 Λ_c track selection

With strict selection criteria set for the final-state hadrons, we now want to restrict how the candidate Λ_c baryon decays. We will study the signal and background distributions for four variables related to the kinematics of the Λ_c track.

- The distance of closest approach (DOCA) is the closest radial separation distance between two particles. For the $\Lambda_c^+ \to p^+K^+K^-$ decay, three DOCA values correspond to the distance between the Λ_c baryon and the three final-state hadrons. The variable Lc_DOCAMAX records the largest of the three DOCA values for each event. Therefore, by restricting Lc_DOCAMAX close to zero, we can ensure that the final-state hadrons originate from the Λ_c baryon.

- The impact parameter (IP) is the perpendicular distance between a particle track and a specified point of origin. The point of origin for all particle decays is the proton-proton collision point, also known as the primary vertex (PV). Shown in Figure 7 is an illustration of the impact parameter with the Λ_c and K^+ particle tracks. The variable Lc_IPCHI2_OWNPV is the measured impact parameter of the Λ_c baryon. From the illustration, we can see that the Λ_c track should have an impact parameter of zero because the particle originates from the primary vertex. Therefore, by restricting Lc_IPCHI2_OWNPV close to zero, we can ensure that the candidate Λ_c comes from the proton-proton collision.

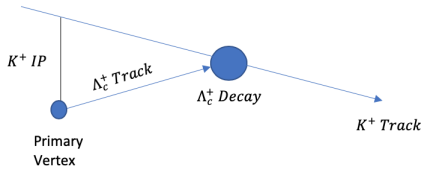

Figure 7: Illustration of the Impact Parameter for the $\Lambda_c^+ \to p^+K^+K^-$ decay involving the Λ_c and K^+ tracks.

- End-Vertex χ^2 represents the quality of the reconstructed decay vertex. For the $\Lambda_c^+ \to p^+K^+K^-$ decay, Lc_ENDVERTEX_CHI2 represents how well the final-state tracks agree with a single decay vertex. Low values of Lc_ENDVERTEX_CHI2 correspond to final-state tracks that intersect at the reconstructed Λ_c decay vertex. By restricting Lc_ENDVERTEX_CHI2 close to zero, we can require that the final-state hadrons came directly from the Λ_c decay.

- Lc_TAU is the measured lifetime of the Λ_c baryon in nanoseconds. The mean lifetime for the Λ_c baryon is (0.2 ± 0.006) picoseconds. Potential peaking backgrounds could still exist due to misidentification of the final-state particles. $D_s^+ \to K^+K^-\pi^+$ and $D^+ \to K^+K^-\pi^+$ events could exist in the data sample if the bachelor π^+ was misidentified as a proton. However, the mean lifetime of the D_s^+ meson is (0.504 ± 0.004) picoseconds and (1.040 ± 0.007) picoseconds for the D^+ meson. Therefore, these potential backgrounds will generally have larger lifetimes, so they could be mitigated by requiring a short decay time.

Figure 8 presents the signal and background distributions for these variables. By setting selection criteria on these four variables, we can remove regions with low signal-to-background ratios. Shown in Table 6 are the selection criteria for the Λ_c track variables.

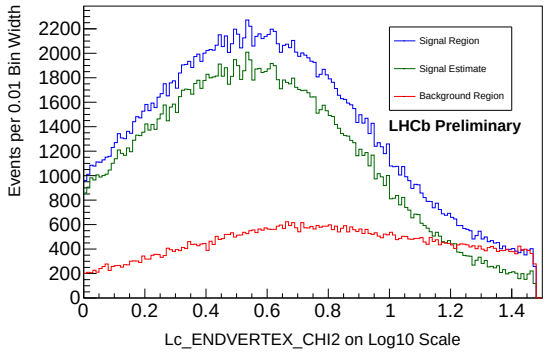

(a) Signal and background distributions of Lc_ENDVERTEX_CHI2.

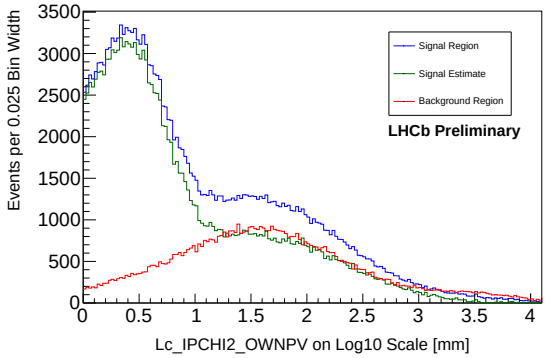

(b) Signal and background distributions of Lc_IPCHI2_OWNPV.

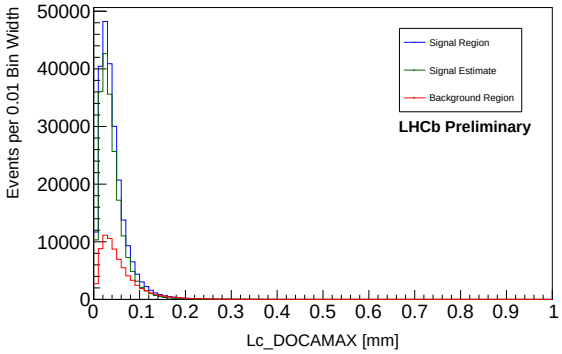

(c) Signal and background distributions of Lc_DOCAMAX.

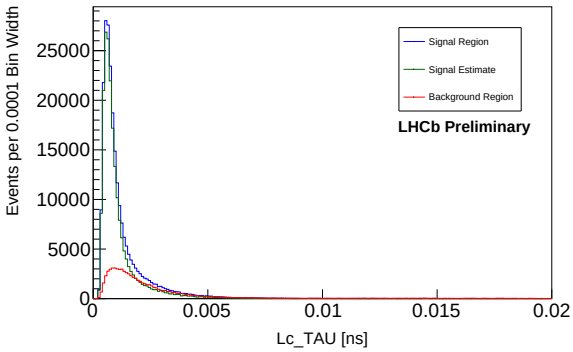

(d) Signal and background distributions of Lc_TAU.

Figure 8: Signal and Background distributions for the Λ_c track variables.

Λ_c Track Cuts	
Variable	Cut
Log10(Lc_ENDVERTEX_CHI2)	< 1.2
Log10(Lc_IPCHI2_OWNPV)	< 1.5
Lc_DOCAMAX	< 0.1 [mm]
Lc_TAU	< 0.02 [ns]

Table 6: Cuts that set strict requirements on Λ_c baryon track and the tracks of its final-state hadrons.

5 Fit Models

Shown in Figure 9 is the resulting Λ_c mass histogram after setting the selection criteria discussed in Section 4. By comparison to Figure 3, the signal to background ratio is far better after applying the selection criteria.

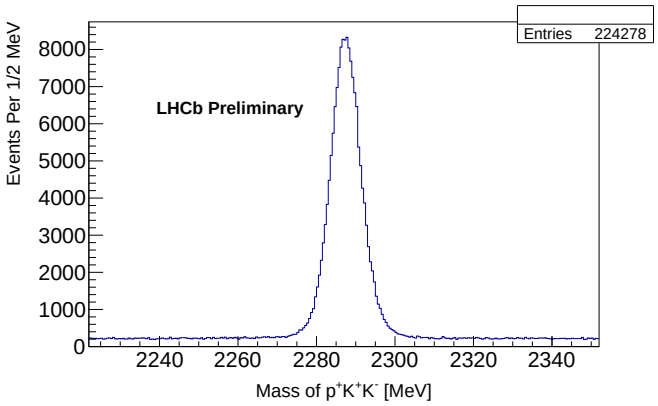

Figure 9: Λ_c mass histogram after applying PID, $\phi(1020)$, and Λ_c track cuts.

We now want to fit the mass histogram with various signal and background models to study the Λ_c mass and its corresponding statistical uncertainty. Shown in Figure 10 is the mass histogram with six different fit models. The statistical uncertainty for all of these fits is 0.011 MeV, and the resulting Λ_c mass values from fitting were consistent with each other. Presented with each of the fit models is a pull distribution. Pull distributions are a visual representation of how accurately the model fits the data in each bin. Low pull values correspond to a fit that closely represents the data. The pull equation depends on the observed value (x), the estimated value (μ), and the error of the observed value (σ)

$$pull = \frac{x - \mu}{\sigma} \tag{1}$$

where for goodness of fit testing, x is the number of events in the bin, μ is the fit value at the center of the bin, and σ is $\sqrt{x}$. In the following subsections, we present each fit and discuss the results. After studying the fit models, we found that the single Gaussian poorly modeled the signal region while the double Gaussian and Crystal Ball fit models were far better. Furthermore, the double Gaussian and Crystal Ball models have very similar pull distributions and signal region parameters, but the Crystal Ball function often fails to converge. Therefore, the double Gaussian fit model has better and more robust results.

5.1 Single Gaussian + linear background

First, we model the data with a single Gaussian signal above a linear background. The equation for this fit model is

$$\frac{N}{\sigma\sqrt{2\pi}} e^{-\frac{(x-\mu)^2}{2\sigma^2}} + b_1 + b_2 x \tag{2}$$

where N is the scaling factor, σ is the standard deviation, μ is the expected value, b_1 is the y intercept of the background, and b_2 is the slope of the background. Figure 10(a) presents this fit with the corresponding pull distribution. The pull plot shows that this fit is a poor representation of the data because it fails to accurately model the tails of the signal region.

5.2 Single Gaussian + quadratic background

Now we want to use the single Gaussian model with a quadratic background. The equation for this fit model is

$$\frac{N}{\sigma\sqrt{2\pi}} e^{-\frac{(x-\mu)^2}{2\sigma^2}} + c_1 - c_2(\mu - x)^2 \tag{3}$$

where c_1 is the height at the μ and and c_2 is the scale for the quadratic background. Figure 10(b) presents this fit with the corresponding pull distribution. Much like the model in section 5.1, this model is a poor representation of the data.

5.3 Double Gaussian + linear background

To account for the tails of the signal region, a second Gaussian function is added to the model. The equation for this fit model is

$$\frac{fN}{\sigma_1\sqrt{2\pi}}e^{-\frac{(x-\mu)^2}{2\sigma_1^2}} + \frac{(1-f)N}{\sigma_2\sqrt{2\pi}}e^{-\frac{(x-\mu)^2}{2\sigma_2^2}} + b_1 + b_2x \tag{4}$$

where f is the fraction of events in the 'first' Gaussian, σ_1 is the standard deviation of the 'first' Gaussian, and σ_2 is the standard deviation of the 'second' Gaussian. Figure 10(c) presents this fit with the corresponding pull distribution. This fit more accurately represents the signal region of the data than of the single Gaussian models. However, there are oscillations in the pull distribution which suggests that another model could be more accurate.

5.4 Double Gaussian + quadratic background

We now fit with a quadratic background to mitigate possible systematic problems with the linear background fit. The equation for this fit model is

$$\frac{fN}{\sigma_1\sqrt{2\pi}}e^{-\frac{(x-\mu)^2}{2\sigma_1^2}} + \frac{(1-f)N}{\sigma_2\sqrt{2\pi}}e^{-\frac{(x-\mu)^2}{2\sigma_2^2}} + c_1 - c_2(\mu-x)^2 \tag{5}$$

Figure 10(d) presents this fit with the corresponding pull distribution. The pull distribution in the background regions is slightly different but not improved.

5.5 Crystal Ball and Gaussian + linear background

To describe long tails within the signal region, we can use a Crystal Ball function. This function is continuous and consists of a Gaussian core stitched together with a power-law tail. Our new function has a Crystal Ball function with a single Gaussian to model the signal region. The equation for this fit model is

$$(1-f)N\begin{cases} e^{-\frac{(x-\mu)^2}{2\sigma_1^2}} & \text{for } \frac{x-\mu}{2\sigma_1} > -\alpha \\ (\frac{n}{|\alpha|})^2 e^{-\frac{|\alpha|^2}{2}}((\frac{n}{|\alpha|}-|\alpha|)-\frac{x-\mu}{\sigma_1})^{-n} & \text{for } \frac{x-\mu}{2\sigma_1} \leq -\alpha \end{cases} + \frac{fN}{\sigma_2\sqrt{2\pi}}e^{-\frac{(x-\mu)^2}{2\sigma_2^2}} + b_1 + b_2x \tag{6}$$

where n and α are fall-off factors for the power-law tail. Figure 10(e) presents this fit with the corresponding pull distribution. Due to the many parameters within this fit model, the parameter limits need to be heavily adjusted. The fit failed to find an appropriate value for the number of signal events, which resulted in a significant error. Furthermore, the resulting μ value is different from the μ value found with the double Gaussian fit model.

5.6 Crystal Ball and Gaussian + quadratic background

Now we try the Crystal Ball and Gaussian fit model with a quadratic background. The equation for this fit model is

$$(1-f)N\begin{cases} e^{-\frac{(x-\mu)^2}{2\sigma_1^2}} & \text{for } \frac{x-\mu}{2\sigma_1} > -\alpha \\ (\frac{n}{|\alpha|})^2 e^{-\frac{|\alpha|^2}{2}}((\frac{n}{|\alpha|}-|\alpha|)-\frac{x-\mu}{\sigma_1})^{-n} & \text{for } \frac{x-\mu}{2\sigma_1} \leq -\alpha \end{cases} + \frac{fN}{\sigma_2\sqrt{2\pi}}e^{-\frac{(x-\mu)^2}{2\sigma_2^2}} + c_1 - c_2(\mu-x)^2 \tag{7}$$

Figure 10(f) presents this fit with the corresponding pull distribution. Unlike the previous fit model, the Crystal Ball and Gaussian with the quadratic background model converged. The resulting μ value has the same μ value as the double Gaussian models. Furthermore, the number of signal events and corresponding errors are more reasonable.

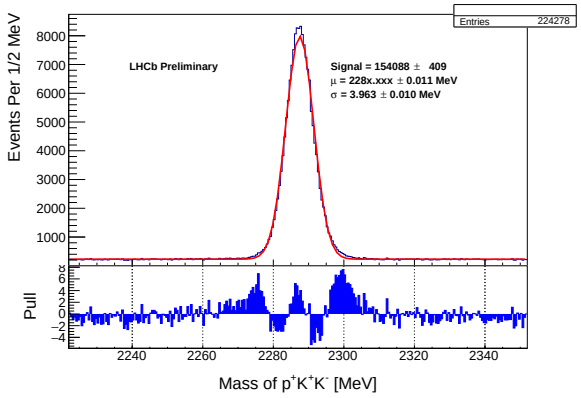

(a) Single Gaussian with linear background

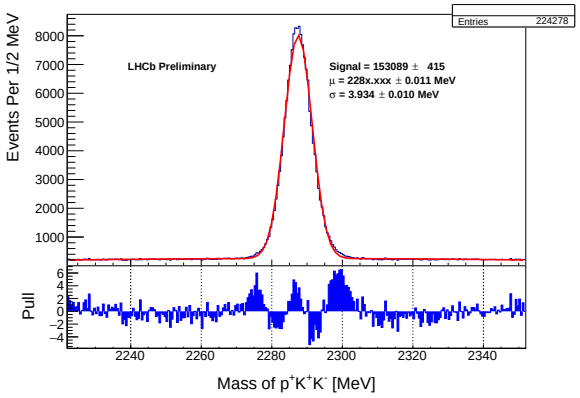

(b) Single Gaussian with quadratic background

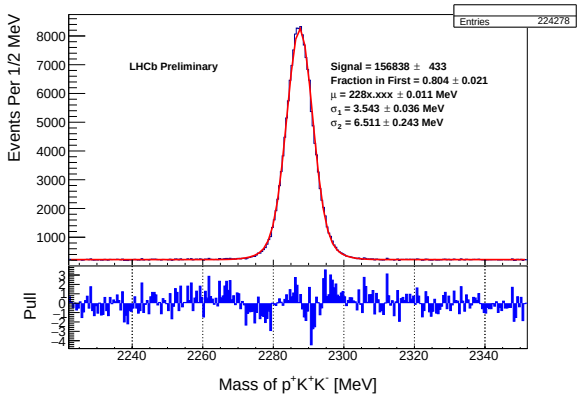

(c) Double Gaussian with linear background

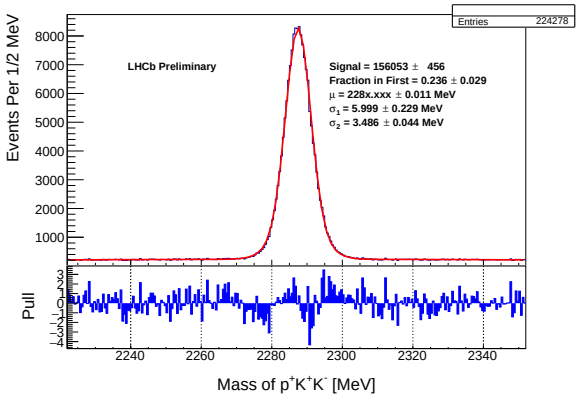

(d) Double Gaussian with quadratic background

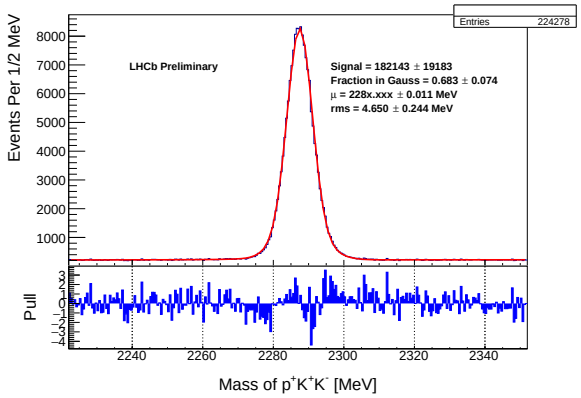

(e) Crystal Ball and Gaussian with linear background

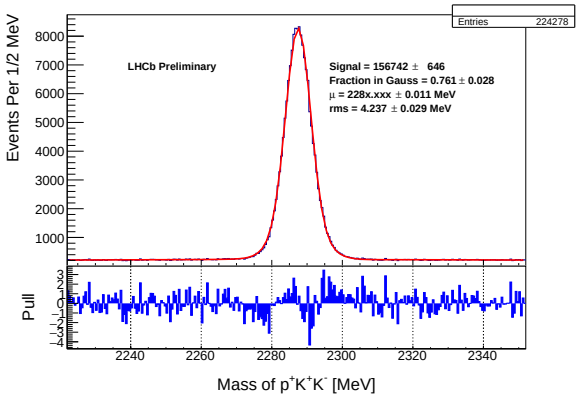

(f) Crystal Ball and Gaussian with quadratic background

Figure 10: Λ_c mass histograms with various fit models.

6 Systematic Uncertainties

With a fit model selected, we study the sources of systematic uncertainties. Systematic uncertainties arise from inefficiencies and imperfections in the LHCb detector. Potential sources of systematic uncertainty are the detector's magnetic field orientation, how the hadron momentum is determined, and whether the candidates were particles or antiparticles. Systematic errors are determined by studying how these detector inefficiencies cause statistical deviations in the Λ_c mass. A powerful dipole magnet generates the magnetic field inside the LHCb detector. If there are discrepancies between the strength and orientation of the magnetic field for the Magnet-Up and Magnet-Down phase, then there will be differences in momentum measurements. Therefore, the Λ_c mass measurement could depend on whether the event occurred during a Magnet-Up or Magnet-Down phase. To attribute a systematic error to the LHCb's magnet, we divide the data into disjoint subsets and study how far each Λ_c mass measurement deviates from the mean value. Shown in Figure 11(a) is a visualization of the mass deviations for the LHCb magnet with the associated error bars and χ^2/NDF. χ^2/NDF is a goodness of fit test evaluated from the measured masses and their associated errors. When $\chi^2/NDF \leq 1$, the detector imperfections are consistent with statistical fluctuation. However, when $\chi^2/NDF > 1$, the measured mass deviations are sources of systematic errors. For systematic error calculations, the χ^2/NDF equation is:

$$\chi^2/NDF = \frac{1}{n}\sum_{i=1}^{n}\frac{(O-E)^2}{\sigma^2} \tag{8}$$

where n is the number of disjoint subsets, $(O-E)$ is the deviation between the measured mass of a subset from the mean measured mass, and σ is the statistical error of the measured mass. A systematic error can be determined from χ^2/NDF through the following equation:

$$\sigma_{sys} = \sigma_{stat}\sqrt{1-\chi^2/NDF} \tag{9}$$

where σ_{stat} is the statistical error found in section 5. Now we can repeat this process for other sources of systematic errors. Shown in Figure 11(b) and Figure 11(c) are the mass deviations for four disjoint Λ_c momentum regions and the charge of the Λ_c candidate. Systematic errors are added in quadrature such that

$$\sigma^2_{sys,total} = \sigma^2_{sys,magnet} + \sigma^2_{sys,momentum} + \sigma^2_{sys,charge} \tag{10}$$

Reported in Table 7 are the χ^2/NDF and error values for the three sources of detector inaccuracies. We found that the deviations from the charge of the particle were consistent with random fluctuation. Therefore, only the momentum regions and magnetic field orientation contribute to the systematic error. After using equations 8, 9, and 10 for the χ^2/NDF values, the total systematic error of the Λ_c mass measurement is $0.05974\,\mathrm{MeV}/c^2$. We must also consider the uncertainties in the mass measurements of the final-state hadrons. The reported proton mass error is $\pm 0.000006\,\mathrm{MeV}/c^2$, and the reported kaon mass error is ± 0.016 MeV. By adding in quadrature the proton and two kaon mass measurement errors, the resulting error is $\pm 0.032\,\mathrm{MeV}/c^2$. Adding in quadrature the statistical error, systematic error, and final-state mass error, the measured Λ_c mass is $228x.xx \pm 0.06865\,\mathrm{MeV}/c^2$.

Systematic Deviations		
Variable	χ^2/NDF	Error
Magnetic Field Orientation	20.9581	$0.0496\,\mathrm{MeV}/c^2$
Λ_c Momentum	9.97851	$0.0333\,\mathrm{MeV}/c^2$
Λ_c Charge	0.002	$0\,\mathrm{MeV}/c^2$

Table 7: χ^2/NDF and error values for the potential sources of systematic uncertainty.

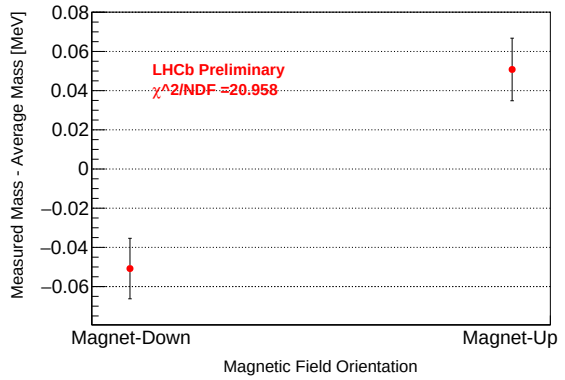

(a) Λ_c mass deviations for different magnetic field orientations.

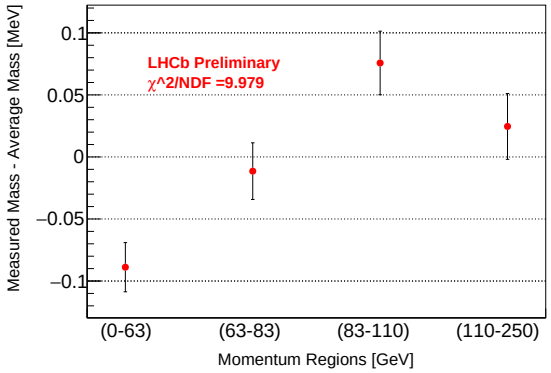

(b) Λ_c mass deviations for different Λ_c momentum regions.

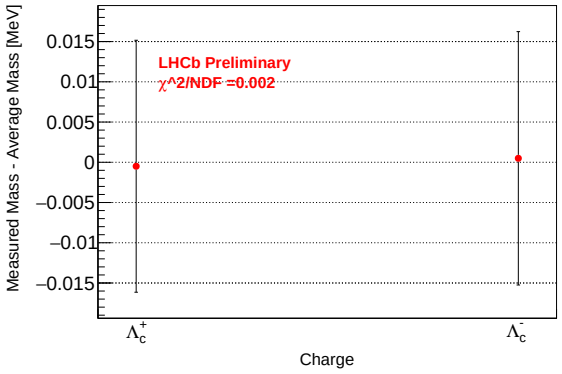

(c) Λ_c mass deviations for different Λ_c charges.

Figure 11: Mass deviation plots for sources of systematic error.

7 Momentum scaling corrections

From section 6, the studies of systematic uncertainties led to the conclusion that systematic deviations between Λ_c mass measurements were the predominant source of error. We now attempt to remedy these systematic errors by calculating momentum scaling correction factors. Before the final-state hadrons enter the second RICH sub-detector, they pass through the outer-tracker. The outer-tracker determines each hadron's position and momentum as they pass through a series of three tracking stations. If these tracker stations incorrectly determine a hadron's momentum due to misalignment, then the Lorentz four-vector for each final-state hadron and the reconstructed Λ_c mass will be inaccurate. Therefore, we can explain the source of systematic errors if a hadron's measured momentum depended on its position within the tracker. We first choose to study this position dependence at the second tracker station to reduce our scope to a 2-dimensional grid. We can then determine correction factors for various position coordinates in the 2-dimensional grid by studying a different decay and assuming that the reconstructed candidate mass should be the expected PDG value. To reduce the systematic error from the magnetic field orientation, we also determine independent correction factors depending on whether data collection occurred during a Magnet-Up or Magnet-Down run. $D^+ \to K^+K^-\pi^+$ is an excellent decay to study because there are large data samples for this decay that already exist. We want to use large data samples to determine correction factors for many positions within the tracker system. Furthermore, the D^+ has a well-known mass and shares similar kinematics to the $\Lambda_c^+ \to p^+K^+K^-$ decay. Now that we have determined Magnet-Up and Magnet-Down correction factors, we can interpolate momentum corrections for the Λ_c final-state hadrons from their positions and the magnetic field orientation. After applying these corrections, we can reconstruct the Λ_c mass from the final-state hadrons' corrected Lorentz four-vectors. Shown in Figure 12 is the Λ_c mass histogram after applying the selection criteria and momentum correction factors with a double Gaussian fit model. Next, we present how well the corrections reduced systematic errors. Shown in Figure 13 are the mass deviation plots for the corrected Λ_c mass. Presented in Table 8 are the corresponding χ^2/NDF and error for each source of systematic uncertainty.

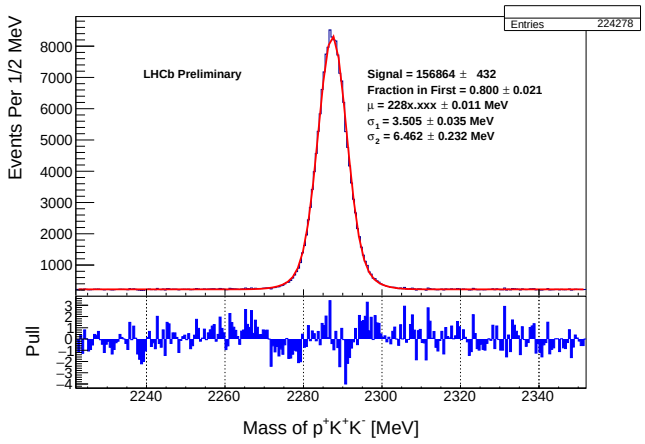

Figure 12: Λ_c mass histogram after cuts and momentum corrections.

Systematic Deviations After Corrections		
Variable	χ^2/NDF	Error
Magnetic Field Orientation	0.866	0 MeV
Λ_c Momentum	11.931	0.0364 MeV
Λ_c Charge	0.130	0 MeV

Table 8: χ^2/NDF and error values for the sources of systematic uncertainty after momentum corrections.

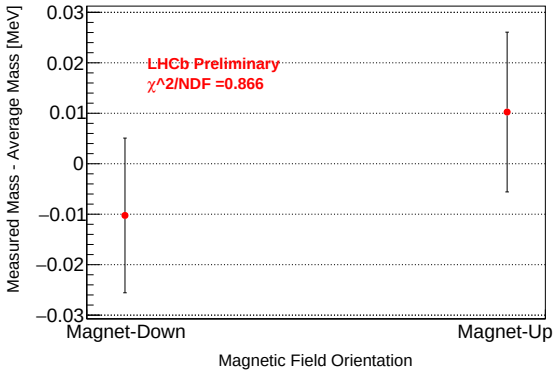

(a) Corrected Λ_c mass deviations for different magnetic field orientations.

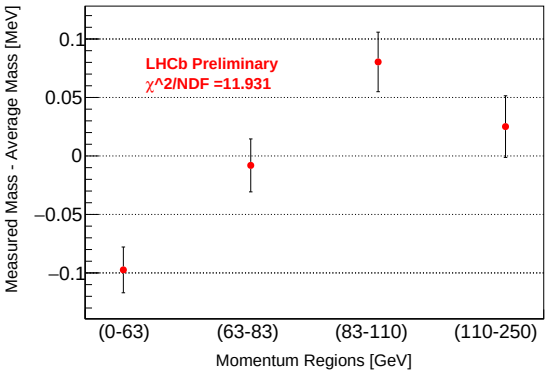

(b) Corrected Λ_c mass deviations for different Λ_c momentum regions.

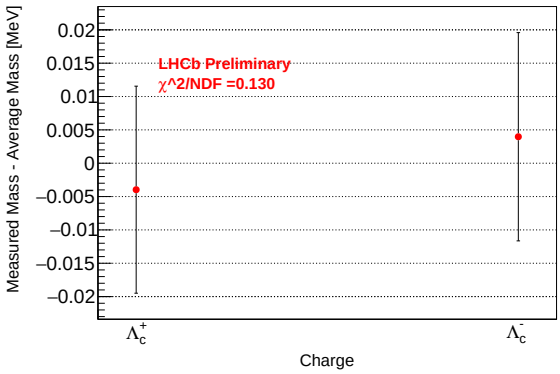

(c) Corrected Λ_c mass deviations for different Λ_c charges.

Figure 13: Mass deviation plots for sources of systematic error.

8 Conclusion

As was expected, the correction factors significantly reduced the deviations between mass measurements for Magnet-Up and Magnet-Down data to the point where the difference is consistent with statistical fluctuation. Mysteriously, the Λ_c mass deviations for different Λ_c momentum regions were nearly unchanged. Further studies are required to determine why the mass dependency on Λ_c momentum persists after final-state hadron momentum corrections. After adding all persisting errors in quadrature, the measured Λ_c mass is $228.xx \pm 0.04969\,\mathrm{MeV}/c^2$. The corresponding error is $0.01910\,\mathrm{MeV}/c^2$ less than the uncorrected Λ_c mass measurement from section 6 and $0.09044\,\mathrm{MeV}/c^2$ less than the current PDG Λ_c mass measurement of $2286.46 \pm 0.14\,\mathrm{MeV}/c^2$ [1]. Further studies of momentum correction uncertainties must be conducted to understand systematic variations. Studies of other sources of systematic uncertainty must also be conducted to more accurately determine the systematic error.

9 Acknowledgement

This work was supported by the National Science Foundation Grant #1806260 through the University of Cincinnati. I would also like to thank Dr. Michael Sokoloff for his guidance and help throughout the project.

References

[1] BABAR collaboration, B. Aubert, *et al., A Precision Measurement of the Λ_c Baryon Mass,* Phys.Rev. (2005) D72:052006, arXiv:hep-ex/0507009

[2] LHC, *Facts and figures about the LHC*
`https://home.cern/resources/faqs/facts-and-figures-about-lhc`

[3] LHCb collaboration, *LHCb - Large Hadron Collider beauty experiment*
`http://lhcb-public.web.cern.ch/`

[4] LHCb collaboration, A.A Alves Jr. *et al., The LHCb detector at the LHC,* JINST **3** (2008) S08005

[5] LHCb collaboration, A. Powell, *Particle Identification at LHCb,* LHCb-PROC-2011-008
textttthttps://cds.cern.ch/record/1322666

[6] LHCb collaboration, A. Wampler, *Search for the purely baryonic decays $B^0_{(s)} \to p\bar{p}p\bar{p}$,* EPFL (2018)

[7] LHCb collaboration, C. Simpson, *Classification of Selection Variables for Rare B-Meson Decays*

[8] Standard Model of Elementary Particles. Courtesy to Wikipedia: 'Standard Model of Elementary Particles' by Cush-Own work by uploader, PBS NOVA, Fermilab, Office of Science, United States Department of Energy, Particle Data Group.